IEEE Access
Multidisciplinary | Rapid Review | Open Access Journal

Received 16 November 2022, accepted 22 November 2022, date of publication 1 December 2022,
date of current version 7 December 2022.

Digital Object Identifier 10.1109/ACCESS.2022.3226248

RESEARCH ARTICLE

Measurement of Construction Materials Properties Using Wi-Fi and Convolutional Neural Networks

MOHAMED A. GACEM[1], (Member, IEEE), AMER S. ZAKARIA[1], (Senior Member, IEEE), MAHMOUD H. ISMAIL[1,2], (Senior Member, IEEE), USMAN TARIQ[1], (Member, IEEE), AND SHERIF YEHIA[3]

[1]Department of Electrical Engineering, American University of Sharjah, Sharjah, United Arab Emirates
[2]Department of Electronics and Communications Engineering, Faculty of Engineering, Cairo University, Giza 12613, Egypt
[3]Department of Civil Engineering, American University of Sharjah, Sharjah, United Arab Emirates

Corresponding author: Amer S. Zakaria (aszakaria@aus.edu)

This work was supported in part by the Faculty Research under Grant FRG20-M-E10, in part by the Master of Science in Electrical Engineering (MSEE) Program, and in part by the Open Access Program at the American University of Sharjah.

ABSTRACT The process of identifying the physical properties of raw construction materials is vital in several industrial and quality assurance applications. Ideally, this process needs to be performed without damaging the sample and at low-cost, while obtaining high-accurate results. In this work, a novel non-destructive construction materials classification tool is proposed. The proposed method is based on passing Wi-Fi signals through the observed samples, then analyzing the Channel State Information (CSI) magnitude and phase components. The collected CSI data packets are pre-processed by performing an averaging operation. Then, the resulting data are divided into training and validation sets and used to train Convolutional Neural Networks (CNNs). Here, the trained CNN models are formulated either as classifiers or regression models, depending on the material under test. If the objective is to sort materials within specific classes, then the CNN is formulated as a classifier. Alternatively, if the goal is to estimate a continuously varying parameter in a material, then the CNN is formulated as a regression model. Furthermore, as per the collected data, the proposed method is used to identify the construction materials based on their thickness, water content value (moisture), and compaction. The obtained experimental results effectively demonstrate the potential and merits of the proposed method. Overall, the trained CNN models achieved a 100% validation accuracy and a low validation loss, which confirms that the method is valid and highly accurate.

INDEX TERMS Channel state information (CSI), classification, construction materials, convolutional neural network (CNN), Wi-Fi sensing.

I. INTRODUCTION

The use of construction materials usually requires performing tests and evaluation procedures to determine the materials' properties and conformity with the safety standards. Several destructive and non-destructive methods are used in the industry to perform such tests. While the destructive methods tend to be more accurate, they are usually costly and impractical to use in applications where the observed material is scarce or when taking a sample would jeopardize the reliability of the structure. Therefore, there is a growing interest in non-destructive construction materials classification methods, since they preserve the observed material's structure while generating reasonably accurate predictions [1], [2]. In this work, we focus on observing and measuring three physical parameters namely, thickness, moisture content, and degree of compaction, in different individual raw construction materials. The conducted experiments were designed to study the internal physical properties of the observed materials, as well as evaluate the proposed method's

The associate editor coordinating the review of this manuscript and approving it for publication was Alberto Cano.

performance robustness to variations in physical traits such as thickness. These parameters have a substantial significance in the industry and quality assurance processes. Furthermore, the existing material classification methods that investigate the mentioned parameters often have a compromise between accuracy, cost, and deployability in practical setups. In the industry, there is considerable interest in measuring the thickness of materials, especially on production lines. Thus, there is a need to develop fast, non-destructive and cost-effective thickness measurement tools. The commonly used techniques include infrared interferometry, X-ray, magnetic induction, Hall effect measurement probes, Eddy-currents, backscattering of beta radiation particles, and the weight gain technique [3]. Each of these methods have their own drawbacks. For example, the Hall effect measurement probes are incapable of measuring opaque materials, and they take a long time to generate results [3]. Furthermore, methods based on radiations, such as X-rays and beta backscattering, pose health and safety risks.

Moreover, in construction, moisture-level monitoring is vital in ensuring the quality and maintaining the performance of raw materials. For example, the surface moisture content measurement of soil is estimated using optical, thermal and satellite remote sensing techniques [4]. Nevertheless, such methods evaluate only the thin upper layer of the soil sample, while not reflecting the moisture content of the internal layers. Furthermore, the estimation of moisture content is widely used in evaluating hardened structures, as to avoid degradation and corrosion; these subsequently lead to cracks and delamination in building structures. Some of the common non-destructive methods for measuring moisture in raw and hardened materials include using embedded humidity sensors with passive RFID tags within the building structure [5], using monostatic radars [6], and measuring the dielectric constant and resistivity [7]. Some of the mentioned techniques require embedding a sensor within the structure, which is not suitable for structures that have specific conductivity and homogeneity requirements. Furthermore, other techniques such as those using gamma rays [8], [9] require a laboratory setup, which limits their use and increases the cost of implementation.

Finally, the estimation of materials' compaction is necessary in some applications for quality inspection. For example, the estimation of asphalt compaction in roads is important as one out of every two defects in asphalt roads is linked to improper compaction [10]. The quality inspection process of asphalt pavement compaction is usually performed by extracting cores from the finished pavement. However, such solution is destructive in nature and results in having potholes in the pavement [11]. Several contributions [11], [12], [13], [14], [15] estimated the compaction of asphalt pavement by studying the vibratory roller's response as it compacts the asphalt mat. As the pavement compaction level increases, the mat becomes stiffer, thus the frequency response of the vibratory roller is altered. Similarly, the authors in [16] estimated the compaction properties of asphalt pavement in real-time, by training an Artificial Neural Network (ANN) using the vibratory response data collected from a uni-axial accelerometer mounted on a vibratory smooth steel drum compactor. However, such method can only be used in the evaluation of pavement asphalt while applying the asphalt layer, and not in later stages. Also, the authors in [17] and [18] suggested a compaction estimation method that relies on the data collected from proctor compaction tests, which involve compacting soil at known moisture contents in a cylindrical mold with a known height and diameter. A compaction curve is then formed by relating the dry density (degree of compaction) to moisture content. Eventually, ANNs and multi-linear regression models were used to estimate the compaction parameters using the compaction curve data. Other compaction estimation methods include using falling weight deflectometer [19] and using ground penetrating radar simulation [20], [21]. However, the accuracy of the latter is affected by the presence of surface moisture.

In this work, a novel non-destructive construction materials classification tool is proposed. The proposed method is based on radiating 2.4 GHz Wi-Fi signals through the observed samples, and then analyzing the signals captured at the receivers. The received data are comprised of the magnitude and phase of the Channel State Information (CSI) for the captured Wi-Fi signals. This technique is based on the fact that the received Wi-Fi signals, and thus CSI data, are affected by the variations in the channel between the transmitter and receiver. Moreover, the placement of different objects in the channel will yield different CSI responses.

After measuring the signals at the receiver, the collected CSI data packets are pre-processed by performing an averaging operation. The resulting processed data are then equally divided into training and testing datasets, and then used to train a Convolutional Neural Networks (CNN). The CNN algorithm can learn the distinctive features of the training data and then classify any new data with high accuracy. The utilized CNN models are formulated either as classifiers or regression models, depending on the material under test. If the objective is to sort the material into classes, then the CNN model is formulated as a classifier. Otherwise, if the objective is to estimate a continuous property of the material, then the CNN is formulated as a regression model. It should be noted here that the CSI data were analyzed using a learning-based algorithm, since this technique has a well-established capability of classifying new data with added variations to a high accuracy. Such a feature is vital for our application, since most measurements are expected to be performed in situ, where the environment constantly changes. Hence, by using a learning-based algorithm, we managed to create a robust system, whose performance can be constantly improved by introducing new training data.

The measurement setup used in this work is composed of commercial off-the-shelf components. The CSI data are collected using ESP32-U [22] development boards with an ESP32 CSI toolkit [23] installed on the computer connected to the receiver. The aforementioned development boards are

widely used in a variety of internet-of-things applications due to their reliability and low cost.

It should be noted here that the presented work focuses on studying individual construction materials that have a uniform homogeneous structure, rather than heterogeneous construction mixtures such as concrete. More specifically, the materials analyzed in this work include Plexiglas, dune sand, crushed sand, 10 mm coarse aggregates, 20 mm coarse aggregates, and cement.

The contributions of this work can thus be summarized as follows:

1) Studying the Wi-Fi CSI response variation in several scenarios: Plexiglas sheets with varying thickness, sand samples with different compactness, and sand mixtures with various water content.
2) Presenting a material classification method based on the captured Wi-Fi CSI data and CNNs. To the best of the authors' knowledge, this is the first work that measures the thickness of Plexiglas as well as the water content and compaction of dune and crushed sand using the proposed method. Furthermore, this method measures three different traits in construction materials using the same hardware and software components, which confirms its versatility and low-cost.
3) Collecting a CSI database for each training scenario. Several variations were introduced to the data collection process to improve the generalization ability of the trained CNN models.

The rest of the paper is organized as follows. Section II summarizes the existing contributions and related work. In Section III, the proposed methodology is explained. In Section IV, the conducted experiments and data collection setup are presented. Subsequently, the obtained results are shared and discussed in Section V. Finally, the conclusion and future work are presented in Section VI.

II. RELATED WORK

The process of evaluating and classifying construction materials is vital in industrial and quality assurance applications. In recent years, significant research work was conducted in the field of destructive and non-destructive evaluation of such materials. In comparison to destructive techniques, the non-destructive evaluation methods have a better edge due to their lower cost, compact size of instruments used, and the fact that the observed samples are kept intact, which is a requirement in several construction scenarios. In this section, the focus is to present work related to nondestructive evaluation techniques for materials. First, the state-of-the-art nondestructive methods for estimating the materials' thickness, moisture content, and compaction level will be reviewed. Then, the related works that uses Wi-Fi for materials' properties estimation are reviewed.

A. THICKNESS ESTIMATION

The weight gain technique is one of the simplest methods to estimate the thickness of a layer, an object or a sample [3]. In this method, the thickness of copper coating is estimated by monitoring the weight of the sample as the coating is applied; the weight of the sample is correlated to the coating thickness. A drawback of this method is that it cannot evaluate the uniformity of the coating process.

Another nondestructive technique, which is utilized in pavement layer thickness measurements, is the ground-penetrating radar. This method is proposed as an alternative to the traditional destructive methods discussed in [24]. In this process, electromagnetic signals are radiated to the pavement, and the reflected echo signals are captured and used to estimate the thickness. The disadvantages of this technique is the complexity of interpreting the results and the lack of reliable automated procedures.

A third technique that is used in estimating the thickness of concrete structures is the use of piezoelectric oscillators placed on the structure itself [25]. The resonance frequency of the oscillators is measured, which is inversely proportional to the concrete thickness. Two drawbacks of this technique is that piezoelectric sensors are prone to get damaged easily, and the sensors themselves need to be placed on the structure, which might be an issue if access to the structure is restrictive.

A fourth method to estimate the materials' thickness is by using infrared thermography as proposed in [26]. In this technique, data captured from thermal cameras are used to generate a one-dimensional heat flow model of the material under test. Then, an elementary theory of one-dimensional heat conduction is used to determine thickness as well as detect flaws. One disadvantage in this technique is that equipment is expensive.

Finally, a fifth method for measuring the thickness of Plexiglas is by building a prediction model as explained in [27]. This model utilizes the dielectric constant of the material, which is measured using the procedure detailed by the National Institute of Standards and Technology (NIST). In this procedure, the scattering parameters are measured and the dielectric constant values are used as inputs for Deep Neural Network (DNN) and Support Vector Machine (SVM) learning algorithms.

B. MOISTURE CONTENT ESTIMATION

A common technique to estimate moisture is by placing electromagnetic sensors within the material structure to measure humidity; the amplitude of the electromagnetic signals from the sensors varies with moisture. For example, the authors in [5] placed humidity sensors with passive high-frequency Radio-Frequency IDentification (RFID) tags within reinforced concrete structures. Similarly, the authors in [28] used a microwave sensor chip embedded within concrete structures to measure the moisture. Drawbacks of this method include the impracticality of placing sensors inside the material for certain structures with complex designs, and the sensors might not perform well if the materials' conductivity is high.

Another technique proposed by the authors in [6] uses continuous-wave monostatic radar to estimate the moisture

content of concrete. In this method, a model is created to correlate the reflection coefficient of the transmitted microwave signals with material's moisture content. Here, the authors observed distinct responses for different moisture content values.

A third technique presented in [7] estimates the moisture content in solid ceramic bricks of historic buildings by performing measurements using dielectric, resistive, and microwaves meters. The initial set of collected data is used for training and validating an ANN, which is then used to estimate the moisture content from newly collected data. While the estimated values from this technique are accurate, the overall cost of its implementation is high due to the use of various meters. Additionally, using three different measurement techniques in one method is impractical and will increase the sources of error.

A fourth approach utilized in [8] and [9] radiates building materials with gamma rays, and measures the amplitude attenuation and the backward angle scattering of the reflections. The measurements are correlated to the moisture content in the materials. Due to the use of ionizing radiation, the equipment needed to conduct the tests needs to be present in a laboratory environment; this limits the usability of this method in practice. In addition, special precautions need to be taken since gamma radiation is utilized.

Finally, a fifth technique for measuring the moisture content of wood is detailed in [29]. Here, Back-propagation (BP) neural network models are trained using real-time measurements of the internal temperature and pressure of wood, the wood's drying time, and the position of the measurement points. A disadvantage here is that these parameters are affected by environmental factors, which impacts the accuracy of the trained models.

C. COMPACTION ESTIMATION

Unlike thickness estimation and moisture content prediction, non-destructive methods to monitor the quality of compaction in construction materials are limited. Examples of these techniques include using ground-penetrating radar to monitor asphalt quality [30] and utilizing ultrasonic pulses to estimate the compaction level of alumina powder [31]. In both these techniques, the reflected signals are correlated with the compaction stage of the materials. Another non-destructive method proposed in [32] and [33] is based on the continuous analysis of parameters measured from the compaction machines during the compaction process itself.

D. WI-FI BASED TECHNIQUES

The use of Wi-Fi signals in sensing applications has gained significant interest in recent years due to the wide use of Wi-Fi in indoor environments and the low-cost of implementation [34]. In Wi-Fi based methods, the experiment involves the presence of a Wi-Fi transmitter and one or more receivers; at the receivers, the magnitude and/or phase of the captured signals are measured. These signals are further processed to observe a phenomenon between the transmitter and receivers. For example, in [35], 2.4 GHz commodity Wi-Fi signals were used to track the motion of humans behind a wall or a closed door. Similar techniques are used to detect abnormal movements associated with Cerebellar dysfunction [36] and to assess Parkinson's disease [37].

In literature, several studies have been conducted on using the CSI data from captured Wi-Fi signals in various applications. For example, Wi-Fi based methods are used to detect the presence of humans [38], [39], [40], [41], detect falling people [42], [43], [44], [45], and detect motion [46], [47], [48], [49]. Furthermore, captured Wi-Fi signals are utilized to recognize human activity [50], [51], [52], [53] as well as recognize gestures [54], [55], [56], [57], and track and classify moving objects [58]. For materials, Wi-Fi sensing experiments are considered to distinguish between metals and insulators [59], [60], [61], [62], estimate the moisture content in wooden samples and wheat [63], [64], and measure the dielectric properties of liquids [65].

A conclusion that can be drawn from literature is that the use of Wi-Fi CSI along with CNN for estimating the thickness, water content, and compaction of building materials has not been previously proposed. Hence, the objective of this work is to address this issue, and propose a low-cost alternative to current non-destructive techniques discussed in preceding sections.

III. METHODOLOGY

In this section, an overview of the methodology followed in this study is presented. As outlined in the previous sections, the three main steps in the proposed classification process are Wi-Fi CSI data collection, data processing, and training CNNs using learning algorithms.

A. CHANNEL STATE INFORMATION

The magnitude and phase of the CSI data from the received Wi-Fi signals capture the effects of signals propagating in a channel. Thus, variations in the channel will lead to magnitude and phase changes.

Furthermore, the Wi-Fi standard makes use of orthogonal frequency division multiplexing, which allows the transmission of several signals in a parallel manner over different subcarriers, or frequencies, within the allocated Wi-Fi channel bandwidth. The CSI is measured by sending a predefined signal, usually a Long Training symbol (LTS), from a Wi-Fi transmitter to a Wi-Fi receiver. This signal gets affected by channel conditions such as fading, dynamic events and objects placed in the channel, in the form of amplitude and phase distortion. Therefore, the relationship between the transmitted and received signal gives an overview of the channel state at a given subcarrier frequency. This results in the following input-output relationship at a given subcarrier frequency f:

$$Y(f) = H(f)X(f) + N(f), \tag{1}$$

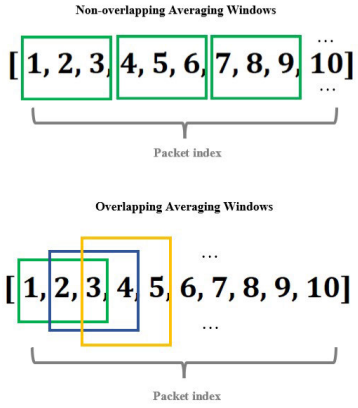

FIGURE 1. Comparison between non-overlapping and overlapping averaging windows. Each number represents a packet.

where $X(f)$ is the transmitted signal, $Y(f)$ is the received signal, $N(f)$ is the additive white Gaussian noise, and $H(f)$ is the complex channel response. The collected CSI data represent the channel response $H(f)$, which in complex form can be written as

$$H(f) = |H(f)| \exp(j\theta), \tag{2}$$

where $|H(f)|$ is the magnitude and θ is the phase of the CSI at frequency f. The effects of fading, scattering, power decay, moving objects, and the type of materials in the channel are captured in the CSI.

B. DATA PROCESSING

In our work, the process of collecting the CSI data involves capturing several CSI packets for each object or material under test. A single CSI packet consists of data at all the subcarriers. After collecting all the packets, this is followed by getting their average; this helps in reducing the effects of noise, and also mitigates the effects of any possible outlier event that might occur in the channel while data recording. Moreover, the size of the averaging window, representing the number of packets that are averaged in this step, determines the number of the resulting training samples and the accuracy of the trained model. More specifically, a smaller averaging window will result in more training examples, but at the cost of having a lower noise suppression performance. The latter could be overcome by using overlapping averaging windows, which makes it possible to have a large number of training examples while averaging numerous packets as shown in Fig. 1.

C. CONVOLUTIONAL NEURAL NETWORK

The processed CSI data are equally divided to train and test a CNN, which will be used to extract the datasets' features and classify them. A CNN is a type of deep learning architecture, which can perform sophisticated classification tasks by learning the distinctive features of several input training examples, and adjusting the weights of the network at the end of each learning iteration based on a defined loss function. This architecture achieves a significantly higher accuracy as compared to traditional neural networks mainly due to the use of convolutional layers, which extract high-level features in the input data to reduce the number of parameters in the model [66].

A CNN consists of an input layer, hidden layers, and an output layer as shown in Fig. 3. The hidden layers contain convolutional, pooling and fully connected layers. The convolutional layers perform convolution operations on specific segments of the input at a time. This operation reduces the total number of parameters in the model and captures the dominant features [67]. Such layers have several *hyper-parameters* that control the training and learning process such as the filter size, the number of strides, and the number of filters. The filter size determines the proportion of input that gets convolved at a time while the number of strides determines the sliding steps of the filtering window during the convolution process [67]. The pooling layers, on the other hand, reduce the number of parameters and the computational cost in the network. The most common pooling operation is max pooling, which calculates the maximum of a set of values in a local neighborhood. Furthermore, it has been observed that max pooling layers help in suppressing the noise present in the input [68]. The extracted features then pass through a flatten layer, which converts the data into a 1-dimensional array to be compatible with the following layers. Once the features are extracted using the previously mentioned layers, the network uses fully connected dense layers with non-linear operations to complete the classification process and generate a prediction. Finally, an error function calculates the model loss, which further updates the weights accordingly [69].

In this work, a categorical cross entropy loss function is used in the classification models while a mean squared error (MSE) function is used in the regression models. The selection process of the appropriate CNN model and loss function is illustrated in the flowchart shown in Fig. 2.

The categorical cross entropy function is particularly used as a loss function in multi-class classification tasks since in such tasks, the training examples and predictions can only belong to a single class. Therefore, by using categorical cross entropy, each training example is labeled with a hard coded vector, which assigns 1 to the correct class, and 0 to the other classes. Each hard coded vector can be considered as a probability distribution. Hence, the output of the model reflects the probability that a training example belongs to a specific class. Some regulation techniques such as *dropout* are applied to speed up the training process and avoid over-fitting. Dropout works by nullifying some node outputs to reduce the dependency between layers.

It should be noted that the CNN model is formulated as a classification model when the data can be segmented into distinct classes, e.g. to determine whether the sample under test is compacted or not. On the other hand, the CNN is formulated as a regression model when the collected data represents a continuously varying parameter in the material under test, such as in the case of estimating a

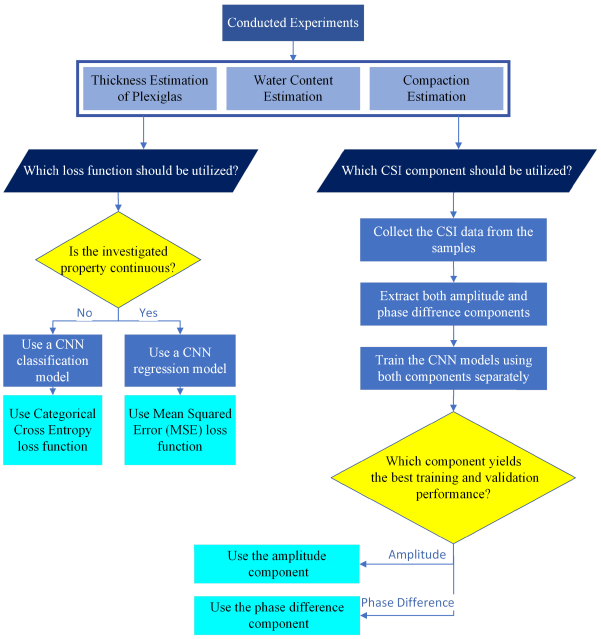

FIGURE 2. A flowchart outlining the decisions on the choice of loss function and the data-type (amplitude or phase) in training the CNN.

sample's thickness or its water content, or moisture, value. The utilized regression models have the same structure as the classification models with the exception of not having an output layer along with using MSE as a loss function.

After training the CNNs, their performance is validated using the testing dataset. In addition, the performance of the regression models used in this work was further validated using k-fold cross-validation. This technique provides a more accurate representation of the validation loss since it alternates between the datasets used for training and validation. It works by dividing the data into k bins, then during the training process one bin is excluded at a time and used for validation [70]. A 5-fold cross-validation is illustrated in Fig. 4. This method ensures that all the CSI packets in the dataset are used at least once for validating the trained models' performance.

IV. EXPERIMENTS AND DATA COLLECTION SETUP

In this section, the CSI data collection setup as well as the experiments done to prepare some of the samples are detailed.

A. CSI DATA COLLECTION SETUPS AND EXPERIMENTS

The CSI data collection setup consists of ESP32-U development boards that are each equipped with patch antennas. One of the boards is used as a transmitter of the Wi-Fi signal, while one or two of the other boards are used as receivers. The ESP32-U development boards are controlled via a computer workstation where the ESP32 CSI toolkit is installed to collect and save the CSI data of the captured signals at the receivers. The process of CSI data collection is initiated after placing the observed sample in the channel between the transmitter and receiving antennas. It was practically observed that attaching the patch antennas directly to the samples resulted in the best performance. The data collection process was performed at the same location several times to ensure the repeatability of the measurements. Additionally, the data were collected from different locations on the same sample to test the learning algorithm's ability to generalize and overcome the variations within the same sample.

The use of one or two receivers is dependent on whether the phase component of the CSI data will be used for training purposes. If only the magnitude of CSI data is used to measure a given parameter, only one receiver is used. If the magnitude as well as the phase are required, the data are captured using two receivers. The phase difference between the signals captured from the two receiving antennas was utilized; it was empirically observed that such relative phase measurement is more accurate than using the phase at one receiver directly. To ensure the proper synchronization of the phase differences, time stamps were associated with the collected CSI packets. The data collection setups using single and two receiving antennas are shown in Fig. 5.

The following should be noted here. It was experimentally observed in the conducted measurements that the CSI amplitude attenuation pattern is not as distinctive as the phase difference pattern. The consequence is a deterioration in the classification performance of CNN if only the amplitude measurements were considered for all the conducted experiments. Hence, in each experiment, the CSI component that yielded the best CNN performance was chosen. The selection process of the CSI component is outlined in Fig. 2.

The experiment conducted for Plexiglas thickness estimation is shown in Fig. 6. A single receiver was used in this experiment, thus only the magnitude of the CSI data was utilized. Moreover, the Plexiglas samples were in the form of sheets, therefore the receiving patch antenna was placed directly on the material under test, while the transmitting antenna was placed 5 cm away since it was experimentally found to generate a better response. The setup is shown in Fig. 6.

The two other experiments performed in this study were data collection to estimate water content and compaction. Two receivers were used, thus both the magnitude and phase components of the CSI data were considered. Moreover, due to the nature of the materials, they were placed in a wooden container as shown in Fig. 7. The size of the box was $30 \times 30 \times 30\ \text{cm}^3$, and the patch antennas were placed directly on the container as shown in the figure.

B. SAMPLES OVERVIEW

In this section, an overview of the properties and dimensions of the samples as well as their preparation process is presented.

1) PLEXIGLAS SAMPLES

In the thickness estimation experiment, the used samples were Plexiglas sheets are stacked together. This formation resembles a real-life application, where Plexiglas sheets are

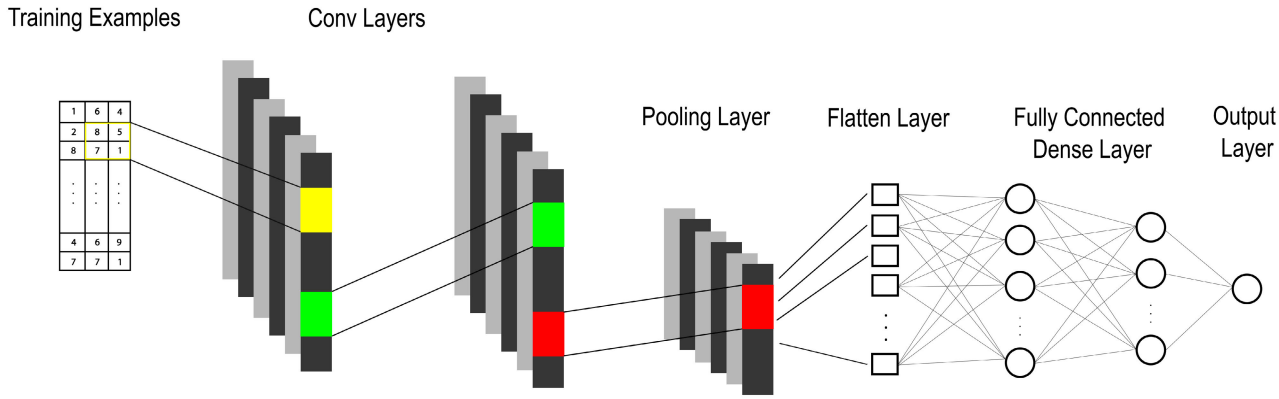

FIGURE 3. CNN classification model architecture.

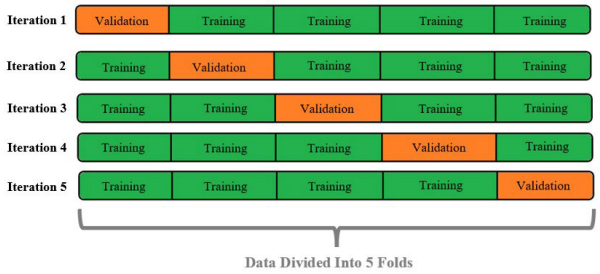

FIGURE 4. 5-Fold cross-validation data segmentation illustration.

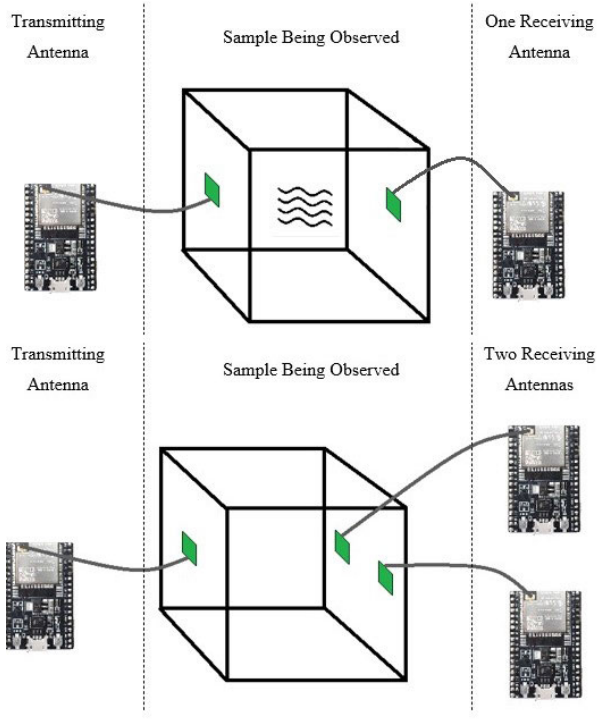

FIGURE 5. Data collection setups using one receiver (up), and two receivers (down).

often stacked in manufacturing lines and in inventory. The CSI data were collected for three different scenarios as stated

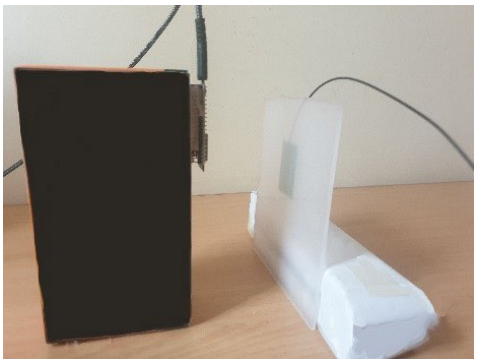

FIGURE 6. Plexiglas data collection experiment.

FIGURE 7. Water content and compaction estimation experiments.

in Table 1 with different number of stacked sheets and consequently, different thicknesses.

2) WATER CONTENT SAMPLES

The moisture estimation experiment requires having samples with specific water content values. The studied samples, whose properties are summarized in Table 2, were dune and

TABLE 1. Plexiglas thickness estimation samples dimensions.

Scenario Number	Number of Stacked Plexiglas Layers	Total Thickness (cm)	Length (cm)	Width (cm)
1	1	0.4	15	15
2	3	1.3	15	15
3	5	2.2	15	15

FIGURE 8. Crushed sand addition of water and mixing process.

crushed sand. The values in the table were obtained from data sheet records shared by the lab that provided the samples.

The process of setting a certain water content value for a sample is achieved using two steps:

1) Water addition: The amount of water X, in liters, needed to achieve a desired water content value C_{desired}, as a percentage, is first calculated as

$$X = T \times C_{\text{desired}}, \tag{3}$$

where T is the total sample weight in kilograms. The calculated amount of water is then added to the sample, and the moist sample is mixed to ensure equal distribution as shown in Fig. 8 for the crushed sand sample.

2) Water content estimation: This step is needed to ensure that the moist material has indeed the desired water content value. This is confirmed by taking a small portion of the sample to perform an oven test, which determines the actual water content. The oven test is widely used in practice to validate the water content value of a specific sample [71]. It involves measuring the sample's weight before and after it being placed in the oven for 24 hours. The following equation is used to obtain the actual water content C_{actual} of the sample:

$$C_{\text{actual}} = \frac{W_{\text{wet}} - W_{\text{dry}}}{W_{\text{dry}}} \times 100\%, \tag{4}$$

where W_{wet} and W_{dry} are, respectively, the weights of the wet and dry samples.

In preparing the samples using dune and crushed sand, the water content was gradually increased until the samples reached saturation. The saturation point was reached when the addition of excess water was seen to rise on the sample's surface. It was observed that dune sand and crushed sand samples reached saturation at 15.8% and 9.9%, respectively. Furthermore, a total of nine moist dune sand samples (2.1%, 4.6%, 6.4%, 8.2%, 9%, 9.9%, 11.1%, 14.2%, 15.8%) and six moist crushed sand samples (2.2%, 4.7%, 4.9%, 7.2%, 8.5%, 9.9%) were studied. For dune sand, the closest separation between the water content values is 0.9%, which is observed between 9% and 9.9%. On the other hand, for crushed sand, the closest separation between the water content values is 0.2%, which is observed between 4.7% and 4.9%. Hence, the water content estimation sensitivity of the proposed method is 0.9% for dune sand and 0.2% for crushed sand.

FIGURE 9. Initial (left) and final (right) compaction stages of dry crushed sand.

3) COMPACTION SAMPLES

For the compaction estimation experiment, both dry and moist samples were studied. The dry samples included dune sand, crushed sand, 10 mm coarse aggregates, 20 mm coarse aggregates, and cement, while the moist ones included the previously aforementioned nine moist dune sand samples, and the six moist crushed sand samples. Therefore, the total number of studied samples was nineteen. The properties of the mentioned materials are summarized in Table 2. A 3-layer compaction process was conducted, where the observed material was placed into the wooden container in three stages. After each stage, the sample was compacted using a ramming hammer. As an example, the initial and final compaction stages of dry crushed sand sample are shown in Fig. 9.

Finally, it is worth mentioning that a total of 17,000 packets were collected per sample in the thickness estimation of Plexiglas experiment, while more than 2,200 packets were collected per sample in the remaining experiments. Furthermore, the number of training examples was expanded by using overlapping averaging windows as mentioned earlier.

V. RESULTS AND ANALYSIS

This section highlights the results obtained from the experiments conducted throughout this work. Again, three

TABLE 2. Properties of samples used in water content and compaction estimation experiments.

Material	Max. Aggregate Size (mm)	Apparent Relative Density	Relative Density on Oven Dried Basis	Relative Density on S.S.D.† Basis	Water Absorption (% by Dry Mass)
Dune Sand	0.3	2.69	2.63	2.65	0.8
Crushed Sand	5	2.69	2.60	2.63	1.3
10 mm Coarse Aggregate	10	2.92	2.86	2.88	0.8
20 mm Coarse Aggregate	20	2.9	2.86	2.87	0.6

†Saturated Surface Dry

experiments were conducted, which were namely, thickness estimation of Plexiglas, water content value estimation, and compaction estimation. The trained CNN classification and regression models' parameters are listed in Table 3. The stated parameters were experimentally varied until the best performance was achieved.

A. THICKNESS ESTIMATION RESULTS

The CSI amplitude data collected from Plexiglas samples with different thicknesses are shown in Fig. 10. The plot shows that samples with different thicknesses have distinctive responses. Indeed, the amplitude gets attenuated as the thickness increases, which is coherent. Therefore, it is expected that the CNN regression models will be able to easily extract the features related to each set of data, since there is no visible overlap or similarity between the sets in the collected data.

The CNN regression models were trained using the parameters listed in Table 3. The training process used an MSE loss function, which represents how far the predicted values are from the actual ones. After 100 epochs, the resulting training and validation losses were 0.0021 and 0.000257, respectively. The plots for the training and validation losses for the first 50 epochs are shown in Fig. 11. The extremely low losses indicate that the proposed method can be used to perform accurate thickness estimation of Plexiglas samples.

The regression models were further verified using the 5-fold cross-validation method. This technique provides a more accurate representation of the validation loss as it alternates between the data used for training and validation as mentioned earlier. The 5-fold cross-validation results are shown in Table 4. These results confirm the validity of the regression model and show that the entire dataset has a consistent set of features with no abnormal data segments.

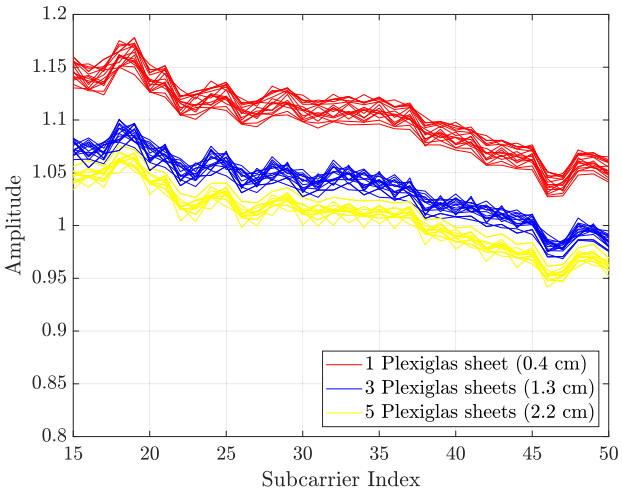

FIGURE 10. Processed CSI amplitude data collected from Plexiglas samples with different thicknesses.

TABLE 3. Trained CNN classification and regression models parameters.

Parameter	Classification Model	Regression Models
Number of Filters	512	32
Size of Filter	4×4	4×4
Number of Neurons in the Hidden Layer	1024	100
Batch Size	16	8
Epochs	100	100
Loss Function	Categorical Cross-entropy	Mean Squared Error (MSE)

The 5-fold cross-validation training loss and validation loss plots are presented in Figs. 12 and 13, respectively.

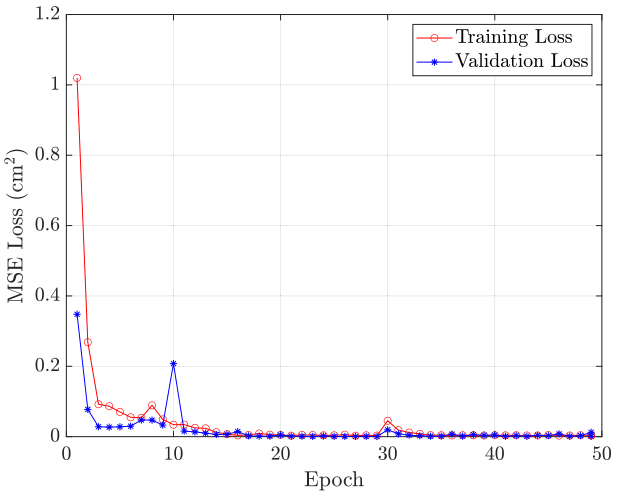

FIGURE 11. Training and validation loss plots for Plexiglas thickness estimation regression model.

TABLE 4. 5-Fold cross-validation results using Plexiglas samples.

Material	Fold Number	Validation Loss	Training Loss
Plexiglas	1	0.00025	0.0010
	2	0.00075	0.0066
	3	0.0037	0.00021
	4	0.0010	0.00065
	5	0.0015	0.00014

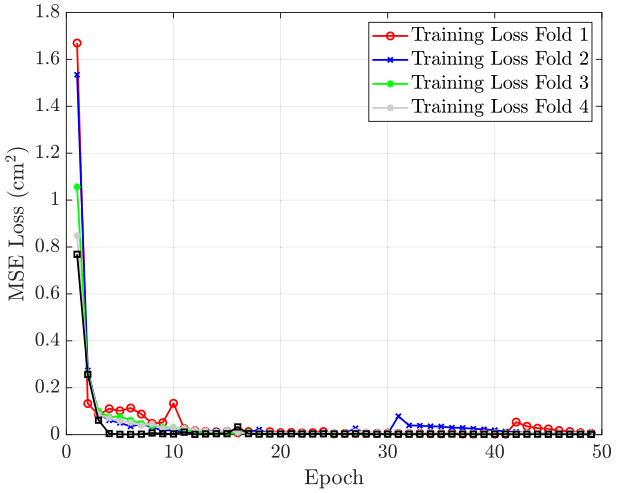

FIGURE 12. Training loss of the CNN model trained on Plexiglas data using 5-fold cross-validation.

B. WATER CONTENT ESTIMATION RESULTS

The CNN models in the water content estimation experiment were formulated as regression models since the percentage of water content in a sample is a continuous variable. The models were trained on a total of nine moist dune sand samples and six moist crushed sand samples; details on the samples were outlined in Section IV-B. Moreover, the training was performed on each sand material, dune and crushed, separately. The regression models were trained using the parameters listed in Table 3.

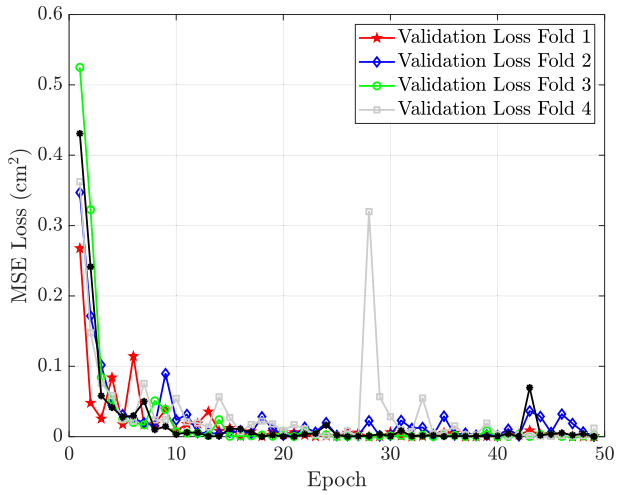

FIGURE 13. Validation loss of the CNN model trained on Plexiglas data using 5-fold cross-validation.

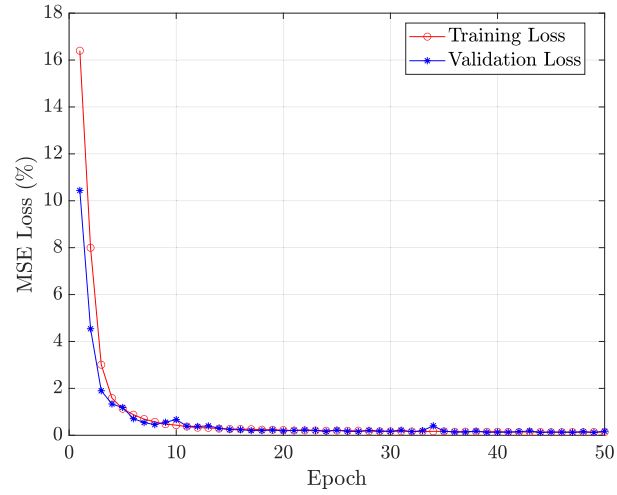

FIGURE 14. Training and validation loss plots for water content estimation in dune sand regression model.

For dune sand, the trained CNN regression model achieved a 0.0902 training loss and 0.0922 validation loss after 100 epochs. Similarly, for crushed sand, the trained CNN regression model achieved a 0.011 training loss and 0.022 validation loss. The low validation loss values indicate that the model can successfully extract the distinctive features from the data. Hence, it can be concluded that the proposed method can be used to estimate the percentage of water content in fine materials such as dune sand and crushed sand. The training loss and validation loss plots after 50 epochs for the dune sand and crushed sand samples are presented in Figs. 14 and 15, respectively.

Similar to Plexiglas thickness estimation, the 5-fold cross-validation technique was applied to verify the models. The 5-fold cross-validation results, presented in Table 5, confirm the previously achieved low validation and training losses;

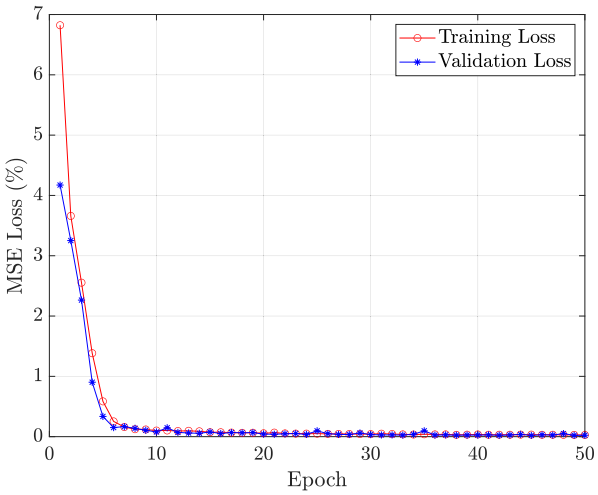

FIGURE 15. Training and validation loss plots for water content estimation in crushed sand regression model.

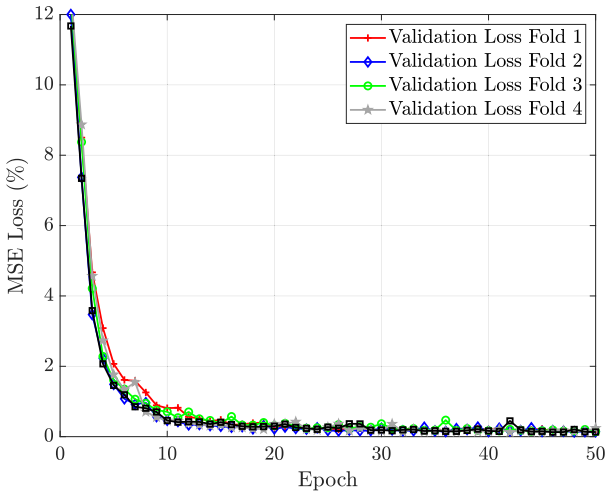

FIGURE 16. Validation loss of the CNN model trained on dune sand data using 5-fold cross-validation.

TABLE 5. 5-Fold cross-validation results for dune sand and crushed sand water content estimation experiment.

Material	Fold Number	Validation Loss	Training Loss
Crushed Sand	1	0.086	0.078
	2	0.085	0.076
	3	0.087	0.077
	4	0.080	0.085
	5	0.082	0.065
Dune Sand	1	0.086	0.081
	2	0.081	0.085
	3	0.14	0.13
	4	0.10	0.090
	5	0.086	0.20

this shows that the entire dataset has a consistent set of features. The 5-fold validation losses plots for dune sand and crushed sand for water content estimation are presented in Figs. 16 and 17, respectively.

Based on the obtained results, it can be concluded that the proposed method can be used to estimate the percentage of water content in dune and crushed sand samples with a 0.9% sensitivity for dune sand and a 0.2% sensitivity for crushed sand.

C. COMPACTION ESTIMATION RESULTS

In the compaction estimation experiment, the CNN models were formulated as classification models and the study was carried on both dry and moist samples as outlined in Section IV-B3. Furthermore, the CSI phase difference component was used in the training of the CNN models. After training, the CNN models were able to distinguish between compacted and uncompacted samples with a 100% validation accuracy. A similar performance was observed whether the samples were dry or moist. The results obtained for the dry and moist samples are given in Tables 6 and 7, respectively.

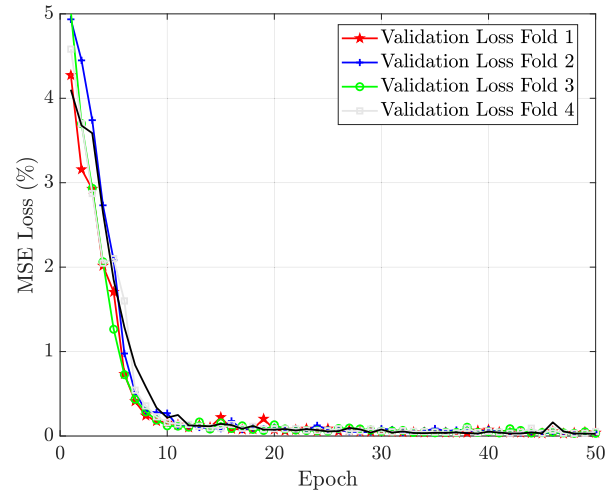

FIGURE 17. Validation loss of the CNN model trained on crushed sand data using 5-fold cross-validation.

TABLE 6. Dry samples compaction estimation results.

Material	Validation Accuracy	Validation Loss	Training Accuracy	Training Loss
Crushed sand	100%	0.031	97.28%	0.086
Dune sand	100%	0.0025	99.91%	0.0076
10 mm coarse aggregate	100%	0.0084	99.27%	0.029
20 mm coarse aggregate	100%	0.0069	100%	0.0050
Cement	100%	0.0015	100%	0.0045

In conclusion, the results show that the proposed method can be used to determine the compaction of individual construction materials. Furthermore, the presence of moisture does not affect the performance of the proposed system.

TABLE 7. Moist samples compaction estimation results.

Material	Validation Accuracy	Validation Loss	Training Accuracy	Training Loss
Crushed sand (2.2%)	100%	0.0035	99.52%	0.031
Crushed sand (4.7%)	100%	0.0025	99.73%	0.0090
Crushed sand (7.2%)	100%	0.00072	100%	0.0022
Crushed sand (9.9%)	100%	0.00092	100%	0.0040
Dune sand (2.1%)	100%	0.0047	99.64%	0.0097
Dune sand (4.6%)	100%	0.0023	100%	0.0046
Dune sand (8.2%)	100%	0.021	99.27%	0.027
Dune sand (9%)	100%	0.0012	99.91%	0.0071
Dune sand (11.1%)	100%	0.013	99.31%	0.022
Dune sand (14.2%)	100%	0.0013	99.91%	0.0075
Dune sand (15.8%)	100%	0.00099	99.46%	0.018

D. ROBUSTNESS ANALYSIS

To further investigate the robustness of the proposed method, two studies were conducted. First, the effect of varying the separation distance between the transmitting (TX) and receiving (RX) antennas was studied. Next, the influence of the surrounding environment is investigated through introducing a conductive object near the setup. These studies were conducted for the Plexiglas sheets thickness estimation experiments, where the CSI amplitude responses were utilized, and the data were collected for three sheets of varying thickness as detailed in Section IV-B.

In the first study, the Plexiglas sheet was placed at an equal distance from the transmitter and receiver antennas, with the transmitter – receiver separation distances varied to 10 cm, 20 cm, and 50 cm as shown in Fig. 19. The CSI amplitude responses collected at different transmitter-receiver separation distances are shown in Figs. 20, 21, and 22. Overall, a total of 13,000 Wi-Fi packets were collected for each thickness value.

Further, for training and testing the CNN models two configurations were considered. In the first, the data for training and testing the CNN models belonged to the datasets of the same TX-RX separation distance. On the other hand, for the second, the data for training and testing belonged to the datasets of different TX-RX separation distances. For example, if a CNN model is trained using the data collected from a 10 cm separation distance, in the first configuration the testing data collected for 10 cm is used for validation, while in the second configuration the testing data collected for either 20 cm or 50 cm separation distances is used for validation. This example is illustrated in Fig. 18

The validation loss results for this study are given in Table 8. The results of the first configuration demonstrate an overall performance consistency of the CNN models when the training and testing data are collected for the same TX-RX separation; this is clear from the table as the MSE values are less than 0.01 for all separation cases. Further, the results for the second configuration give insight into the generalization

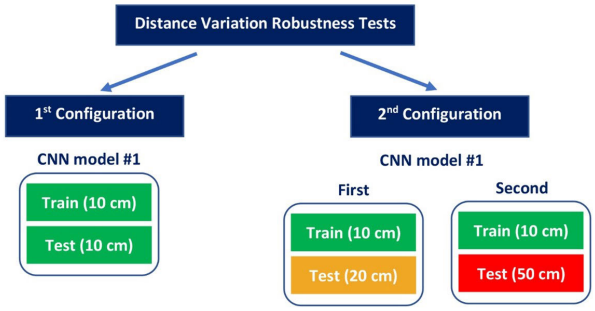

FIGURE 18. Training and testing configurations for distance variation robustness tests.

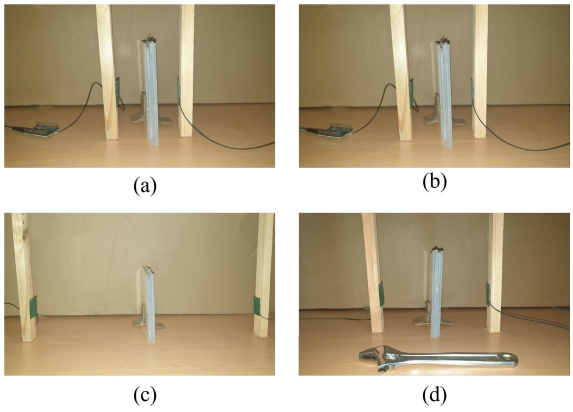

FIGURE 19. Several configurations for testing the robustness of the proposed technique: (a) 10 cm, (b) 20 cm, (c) 50 cm separation between the transmitter and receiver, and (d) placing a conductive object near the setup.

ability of the trained CNN models. Generally, the validation losses are higher as can be observed in Table 8. Nevertheless, for all except one of the validation tests, the MSE values were lower than 0.6. This indicates that the hybrid Wi-Fi CSI-CNN method was able to capture and extract the most distinctive features of the observed objects without being significantly affected by varying the location of the Wi-Fi transducers.

For the second study, a conductive object (metallic wrench) was placed near the data collection setup as shown in Fig. 19. While introducing a conductive object near the setup made the CSI amplitude responses less distinctive, as shown in Fig. 23, the performance of the CNN model achieved a low validation loss of 0.0019.

Based on the results of the studies, the recommendations are to keep the separation between the transmitter and receiver less than 10 cm, and to clear the setup surroundings from conductive objects. This would ensure optimum performance.

E. EVALUATION OF THE 5-FOLD CROSS VALIDATION PROCEDURE

A similar performance from all 5 folds in a 5-fold cross validation test would indicate that the dataset is consistent

TABLE 8. Validation losses for distance variation robustness tests.

Training Data TX-RX Separation Distance	10 cm			20 cm			50 cm		
Testing Data TX-RX Separation Distance	10 cm	20 cm	50 cm	10 cm	20 cm	50 cm	10 cm	20 cm	50 cm
Validation Loss (MSE)	0.001	0.42	0.55	0.54	0.0029	0.54	0.54	1.57	0.0086

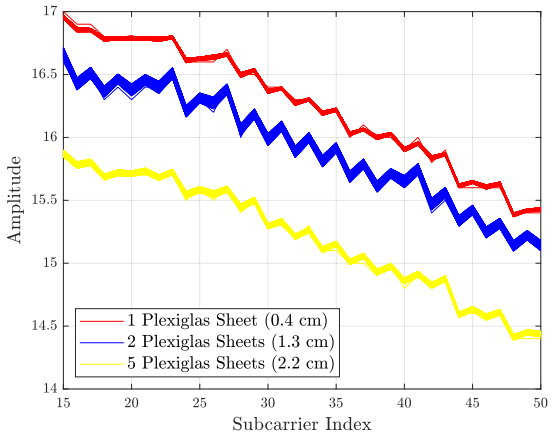

FIGURE 20. The CSI amplitude responses of the three Plexiglas sheets with a separation distance of 10 cm.

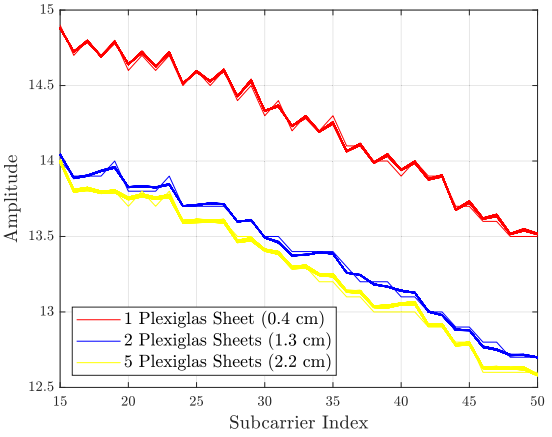

FIGURE 22. The CSI amplitude responses of the three Plexiglas sheets with a separation distance of 50 cm.

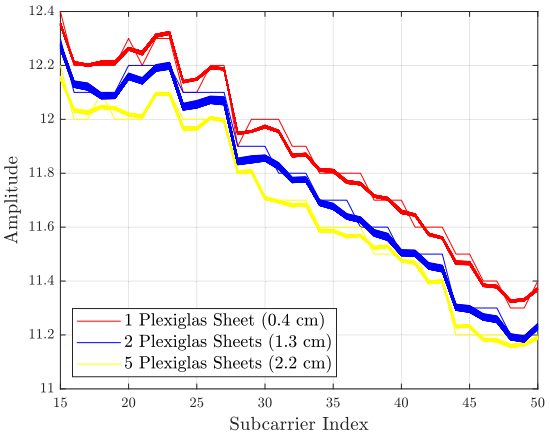

FIGURE 21. The CSI amplitude responses of the three Plexiglas sheets with a separation distance of 20 cm.

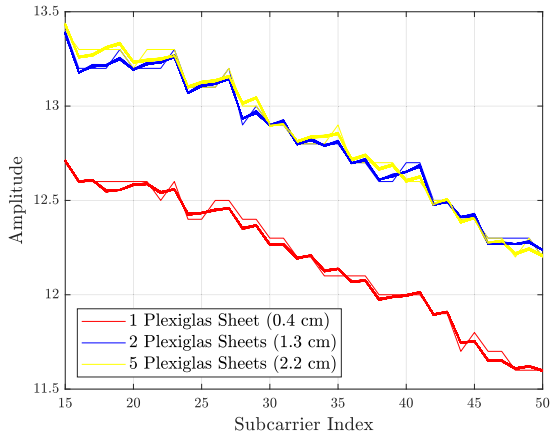

FIGURE 23. The CSI amplitude responses of the three Plexiglas sheets with a conductive object placed near the setup.

and has no abnormal data segments. The performance similarity is evaluated by calculating the coefficient of variation (CV) of the error data resulting from the cross-validation process. The coefficient of variation reflects how the error data are dispersed relative to the mean, and is calculated as,

$$\mathrm{CV} = \frac{\sigma}{\mu} \tag{5}$$

where σ is the standard deviation, and μ is the mean of the error data. A coefficient of variation greater than one would indicate that the model is overfitting or having abnormal data segments. The resulting CV values of all the cross-validation tests conducted throughout the paper, achieved a score less than one as shown in Table 9, which confirms the dataset's consistency and the trained models' generalization ability.

F. PERFORMANCE COMPARISON WITH OTHER SUPERVISED LEARNING ALGORITHMS

To illustrate the merits of using the proposed hybrid Wi-Fi CSI-CNN system over the alternative supervised learning methods, we compared its performance to that obtained using two other supervised learning algorithms namely,

TABLE 9. Coefficient of variation values for the 5-Fold cross validation tests.

Experiment	Standard Deviation (σ)	Mean (μ)	CV
Thickness estimation of Plexiglas	0.0012	0.00144	0.833
Measurement of moisture content in crushed sand	0.002608	0.084	0.031
Measurement of moisture content in dune sand	0.021648	0.0986	0.219

TABLE 10. Thickness estimation of plexiglas experiment evaluation using CNN, ANN, and SVM.

Experiment	Configuration	Learning Algorithm	MSE Validation Loss
Thickness estimation of Plexiglas	Sensors' separation distance = 10 cm	CNN	0.0010
		ANN	0.0051
		SVM	0.022
	Sensors' separation distance = 20 cm	CNN	0.0029
		ANN	0.024
		SVM	0.42
	Sensors' separation distance = 50 cm	CNN	0.0086
		ANN	0.0143
		SVM	0.1649
	Placing a conductor near the setup	CNN	0.0019
		ANN	0.5103
		SVM	0.558

an Artificial Neural Network (ANN) and a Support Vector Machine (SVM) algorithm. An ANN is a supervised learning algorithm, which consists of an input layer, a hidden layer, and an output layer. Each layer consists of neurons, which represent activation functions that perform non-linear operations on the data. ANN are often referred to as Feed-Forward networks since the data are sent in one direction from the input towards the output. On the other hand, an SVM algorithm is a supervised learning algorithm that finds a hyperplane or a decision boundary between data points. The main objective of this algorithm is to find the optimum hyperplane, which yields the maximum margin distance between the data points [72].

In the conducted experiments, the ANN model had 32 neurons in the hidden layer, each using a Rectified Linear Unit (ReLU) activation function, which is commonly used since it reduces computational cost and training time. As for the SVM regression model, a Radial Basis Function (RBF) was set as a kernel function, which is an SVM hyper-parameter that allows the algorithm to deal with higher dimensional space that has linearly inseparable data. Since the CSI data consist of 64 different subcarriers responses, hence 64 dimensional features, it was vital to use the RBF kernel to deal with the high dimensionality.

TABLE 11. Moisture content measurement experiment evaluation using CNN, ANN, and SVM.

Experiment	Learning Algorithm	MSE Validation Loss
Measurement of Moisture Content Crushed Sand	CNN	0.022
	ANN	0.017
	SVM	0.060
Measurement of Moisture Content Dune Sand	CNN	0.092
	ANN	0.12
	SVM	0.15

A comparison of the validation losses of the thickness estimation of Plexiglas and moisture content measurement of dune sand and crushed sand experiments are listed in Tables 10 and 11, respectively. In the thickness estimation of Plexiglas experiment, it can be observed from Table 10 that the proposed CNN algorithm generally outperformed the other two techniques. This could be attributed to the presence of convolutional layers in the CNN that help in extracting the most distinctive high-level features, especially in datasets affected by environment distortions, where the CNN algorithm's performance was by far the best. In the moisture content measurement experiments, both the CNN and ANN achieved a comparable performance, while the SVM recorded the highest MSE loss as can be seen in Table 11. Hence, the hybrid use of Wi-Fi CSI and CNN is found to be the most suitable technique for the applications addressed in this work.

VI. CONCLUSION

In this work, a novel non-destructive construction materials classification tool is proposed. The proposed method is based on collecting the CSI data of Wi-Fi signals, with the material under test being placed in the channel between the transmitter and the receiver. The collected data are processed using an averaging operation to reduce the effect of noise and outlier packets. Then, the pre-processed CSI data are used to train a CNN formulated as classifier or regression model depending on the data type.

The proposed method was used to classify construction materials based on three parameters: thickness, percentage of water content, and compaction. The trained CNN models in all experiments achieved either a 100% validation accuracy with a low validation loss or very small MSE in regression experiments. To the best of the authors' knowledge, this is the first work to use Wi-Fi CSI and CNN in the estimation of thickness, moisture content and compaction of construction materials. Moreover, the mentioned properties were measured using the same hardware and software components, and were found to be robust under different

scenarios and environments; this demonstrates the proposed method's efficiency and viability.

ACKNOWLEDGMENT

The authors would like to acknowledge the generous help provided by the Sharjah Municipality Construction Laboratory for providing them access to their laboratories and for their invaluable assistance in samples preparation.

DISCLAIMER

This paper represents the opinions of the authors and does not mean to represent the position or opinions of the American University of Sharjah.

REFERENCES

[1] S. Farrag, S. Yehia, and N. Qaddoumi, "Investigation of mix-variation effect on defect-detection ability using infrared thermography as a nondestructive evaluation technique," *J. Bridge Eng.*, vol. 21, no. 3, Mar. 2016, Art. no. 04015055.
[2] S. Yehia, N. Qaddoumi, S. Farrag, and L. Hamzeh, "Investigation of concrete mix variations and environmental conditions on defect detection ability using GPR," *NDT &E Int.*, vol. 65, pp. 35–46, Jul. 2014.
[3] F. Haider, M. H. Ani, and M. H. Mahmood, "A comparison between destructive and non-destructive techniques in determining coating thickness," in *Proc. IOP Conf. Mater. Sci. Eng.*, vol. 290, no. 1, Jan. 2018, Art. no. 012020.
[4] L. Wang and J. Qu, "Satellite remote sensing applications for surface soil moisture monitoring: A review," *Frontiers Earth Sci. China*, vol. 3, no. 2, pp. 237–247, Jan. 2009.
[5] C. Strangfeld, S. Johann, M. Müller, and M. Bartholmai, "Embedded passive RFID-based sensors for moisture monitoring in concrete," in *Proc. IEEE SENSORS*, Oct. 2017, pp. 1–3.
[6] K. Haddadi and T. Lasri, "CW radar for monitoring water-to-cellular concrete," in *Proc. 11th Eur. Radar Conf.*, 2014, pp. 529–532.
[7] A. Goetzke-Pala, J. Hoła, and Ł. Sadowski, "Non-destructive neural identification of the moisture content of saline ceramic bricks," *Construct. Building Mater.*, vol. 113, pp. 144–152, Jun. 2016.
[8] A. S. Guimarães, J. M. P. Q. Delgado, V. P. de Freitas, and A. C. Azevedo, "Moisture measuring device based on non-destructive method of gamma ray's attenuation," *Defect Diffusion Forum*, vol. 380, pp. 55–59, Nov. 2017.
[9] D. Bucurescu and I. Bucurescu, "Non-destructive measurement of moisture in building materials by Compton scattering of gamma rays," *Romanian Rep. Phys.*, vol. 63, no. 1, pp. 61–75, 2011.
[10] P. Georgiou and A. Loizos, "A practical non-destructive testing based approach to improve the quality of the asphalt compaction process," in *Bearing Capacity Roads, Railways Airfields*. Boca Raton, FL, USA: CRC Press, 2017, pp. 813–818.
[11] D. Singh, F. Beainy, S. Commuri, and M. Zaman, *Application of Intelligent Compaction Technology for Estimation of an Effective Modulus for a Multilayered Asphalt Pavement*. Reston, VA, USA: ASCE, 2014, pp. 51–58.
[12] S. Commuri, A. Mai, and M. Zaman, "Calibration procedures for the intelligent asphalt compaction analyzer," *J. Test. Eval.*, vol. 37, no. 5, pp. 454–462, 2009, doi: 10.1520/JTE003110.
[13] X. M. Ying, D. F. Zhang, Q. Y. Li, and L. C. Meng, "Research on cement concrete bridge asphalt pavement compaction technology," in *Silicate Building Materials* (Key Engineering Materials), vol. 599. Switzerland: Trans Tech Publications Ltd, 2014, pp. 224–229, doi: 10.4028/www.scientific.net/KEM.599.224.
[14] R. T. Emelyanov, A. P. Prokopev, Y. V. Vasiliev, D. I. Perebeynos, and V. S. Novruzov, "Comprehensive control method of asphalt concrete compaction by road roller," *J. Phys., Conf.*, vol. 1889, no. 4, Apr. 2021, Art. no. 042059.
[15] Z. Xue, W. Cao, S. Liu, F. Ren, and Q. Wu, "Artificial neural network-based method for real-time estimation of compaction quality of hot asphalt mixes," *Appl. Sci.*, vol. 11, no. 15, p. 7136, Aug. 2021.
[16] S. A. Imran, M. Barman, S. Commuri, M. Zaman, and M. Nazari, "Artificial neural network–based intelligent compaction analyzer for real-time estimation of subgrade quality," *Int. J. Geomech.*, vol. 18, no. 6, Jun. 2018, Art. no. 04018048.
[17] O. Sivrikaya and T. Y. Soycan, "Estimation of compaction parameters of fine-grained soils in terms of compaction energy using artificial neural networks," *Int. J. Numer. Anal. Methods Geomech.*, vol. 35, no. 17, pp. 1830–1841, Dec. 2011.
[18] O. Günaydın, "Estimation of soil compaction parameters by using statistical analyses and artificial neural networks," *Environ. Geol.*, vol. 57, no. 1, pp. 203–215, Mar. 2009.
[19] R. Ishikura, S. Fujiwara, and N. Yasufuku, "An estimation method of degree of compaction on embankment slope using the non-destructive testing method," in *Proc. 16th Asian Regional Conf. Soil Mech. Geotechnical Eng. (ARC)*, 2020, pp. 1–4.
[20] P. Shangguan, I. L. Al-Qadi, and S. Lahouar, "Pattern recognition algorithms for density estimation of asphalt pavement during compaction: A simulation study," *J. Appl. Geophys.*, vol. 107, pp. 8–15, Aug. 2014.
[21] S. Wang, S. Zhao, and I. L. Al-Qadi, "Real-time density and thickness estimation of thin asphalt pavement overlay during compaction using ground penetrating radar data," *Surveys Geophys.*, vol. 41, pp. 431–445, May 2020.
[22] (2021). *ESP32, Wi-Fi and Bluetooth, MCU I Espressif Systems*. [Online]. Available: https://www.espressif.com/en/products/socs/esp32/
[23] S. M. Hernandez and E. Bulut. (2021). *ESP32 CSI Toolkit*. [Online]. Available: https://stevenmhernandez.github.io/ESP32-CSI-Tool/
[24] Q. Li, Z. Xia, J. Shao, J. Chen, X. Liu, and G. Fang, "Non-destructive survey of pavement layer thicknesses with ground penetrating radar," in *Proc. IEEE Int. Conf. IEEE Region 10th (TENCON)*, Oct. 2013, pp. 1–4.
[25] M. Pokorny, N. Jendzelovsky, and L. Konecna, "Determination of the dynamic modulus of elasticity and the thickness of concrete structures by non-destructive methods," *Key Eng. Mater.*, vol. 691, pp. 344–355, May 2016.
[26] S. D. Holland and R. S. Reusser, "Material evaluation by infrared thermography," *Annu. Rev. Mater. Res.*, vol. 46, pp. 287–303, Jul. 2016.
[27] P.-T. Hien and I.-P. Hong, "Material thickness classification using scattering parameters, dielectric constants, and machine learning," *Appl. Sci.*, vol. 11, no. 22, Nov. 2021, Art. no. 10682.
[28] K. Teng, P. Kot, M. Muradov, A. Shaw, K. Hashim, M. Gkantou, and A. Al-Shamma'a, "Embedded smart antenna for non-destructive testing and evaluation (NDT&E) of moisture content and deterioration in concrete," *Sensors*, vol. 19, no. 3, p. 547, Jan. 2019.
[29] H. Chai, X. Chen, Y. Cai, and J. Zhao, "Artificial neural network modeling for predicting wood moisture content in high frequency vacuum drying process," *Forests*, vol. 10, no. 1, p. 16, Dec. 2018.
[30] S. Zhao and I. L. Al-Qadi, "Algorithm development for real-time thin asphalt concrete overlay compaction monitoring using ground-penetrating radar," *NDT & E Int.*, vol. 104, pp. 114–123, Jun. 2019.
[31] T. Kathrina and R. Rawlings, "Ultrasonic non-destructive evaluation of alumina powder during compaction," *Brit. Ceram. Trans.*, vol. 95, no. 6, pp. 233–240, 1996.
[32] A. P. Prokopev, Z. I. Nabizhanov, R. T. Emelyanov, and V. I. Ivanchura, "Concept of a new method for continuous non-destructive control of asphalt road pavements compaction," *J. Phys., Conf.*, vol. 1515, no. 5, Apr. 2020, Art. no. 052054.
[33] A. P. Prokopev, Z. I. Nabizhanov, V. I. Ivanchura, and R. T. Emelyanov, "Modeling the non-destructive control of road surfaces compaction," *J. Phys., Conf.*, vol. 1399, no. 4, Dec. 2019, Art. no. 044094.
[34] Y. Ma, G. Zhou, and S. Wang, "WiFi sensing with channel state information: A survey," *ACM Comput. Surv.*, vol. 52, no. 3, pp. 1–36, Jul. 2019.
[35] F. Adib and D. Katabi, "See through walls with WiFi!" in *Proc. ACM SIGCOMM Conf. SIGCOMM*, Aug. 2013, pp. 75–86.
[36] X. Yang, S. A. Shah, A. Ren, D. Fan, N. Zhao, S. Zheng, W. Zhao, W. Wang, P. J. Soh, and Q. H. Abbasi, "*S*-band sensing-based motion assessment framework for cerebellar dysfunction patients," *IEEE Sensors J.*, vol. 19, no. 19, pp. 8460–8467, Aug. 2018.
[37] X. Yang, L. Guan, Y. Li, W. Wang, Q. Zhang, M. U. Rehman, and Q. H. Abbasi, "Contactless finger tapping detection at C-band," *IEEE Sensors J.*, vol. 21, no. 4, pp. 5249–5258, Feb. 2020.
[38] E. Soltanaghaei, A. Kalyanaraman, and K. Whitehouse, "Peripheral Wi-Fi vision: Exploiting multipath reflections for more sensitive human sensing," in *Proc. 4th Int. Workshop Phys. Analytics (WPA)*, 2017, pp. 13–18.
[39] F. Xiao, X. Xie, H. Zhu, L. Sun, and R. Wang, "Invisible cloak fails: CSI-based passive human detection," in *Proc. 1st Workshop Context Sens. Activity Recognit.*, 2015, pp. 19–23.

[40] H. Zhu, F. Xiao, L. Sun, R. Wang, and P. Yang, "R-TTWD: Robust device-free through-the-wall detection of moving human with WiFi," *IEEE J. Sel. Areas Commun.*, vol. 35, no. 5, pp. 1090–1103, May 2017.
[41] Z. Zhou, Z. Yang, C. Wu, L. Shangguan, and Y. Liu, "Omnidirectional coverage for device-free passive human detection," *IEEE Trans. Parallel Distrib. Syst.*, vol. 25, no. 7, pp. 1819–1829, Jul. 2013.
[42] Y. Wang, K. Wu, and L. M. Ni, "WiFall: Device-free fall detection by wireless networks," *IEEE Trans. Mobile Comput.*, vol. 16, no. 2, pp. 581–594, Feb. 2016.
[43] S. Palipana, D. Rojas, P. Agrawal, and D. Pesch, "FallDeFi: Ubiquitous fall detection using commodity Wi-Fi devices," *Proc. ACM Interact., Mobile, Wearable Ubiquitous Technol.*, vol. 1, no. 4, pp. 1–25, Dec. 2018.
[44] F. Zhang, C. Chen, B. B. Wang, and K. J. R. Liu, "WiSpeed: A statistical electromagnetic approach for device-free indoor speed estimation," *IEEE Internet Things J.*, vol. 5, no. 3, pp. 2163–2177, Jun. 2018.
[45] H. Wang, D. Zhang, Y. Wang, J. Ma, Y. Wang, and S. Li, "RT-Fall: A real-time and contactless fall detection system with commodity WiFi devices," *IEEE Trans. Mobile Comput.*, vol. 16, no. 2, pp. 511–526, Feb. 2016.
[46] L. Gong, W. Yang, D. Man, G. Dong, M. Yu, and J. Lv, "WiFi-based real-time calibration-free passive human motion detection," *Sensors*, vol. 15, no. 12, pp. 32213–32229, 2015.
[47] J. Liu, L. Wang, L. Guo, J. Fang, B. Lu, and W. Zhou, "A research on CSI-based human motion detection in complex scenarios," in *Proc. IEEE 19th Int. Conf. e-Health Netw., Appl. Services (Healthcom)*, Oct. 2017, pp. 1–6.
[48] Y. Gu, J. Zhan, Y. Ji, J. Li, F. Ren, and S. Gao, "MoSense: An RF-based motion detection system via off-the-shelf WiFi devices," *IEEE Internet Things J.*, vol. 4, no. 6, pp. 2326–2341, Dec. 2017.
[49] Y. Xu, W. Yang, J. Wang, X. Zhou, H. Li, and L. Huang, "WiStep: Device-free step counting with WiFi signals," *Proc. ACM Interact. Mobile Wearable Ubiquitous Technol.*, vol. 1, no. 4, pp. 1–23, Jan. 2018.
[50] S. Duan, T. Yu, and J. He, "WiDriver: Driver activity recognition system based on WiFi CSI," *Int. J. Wireless Inf. Netw.*, vol. 25, no. 2, pp. 146–156, Jan. 2018.
[51] M. De Sanctis, E. Cianca, S. Di Domenico, D. Provenziani, G. Bianchi, and M. Ruggieri, "WIBECAM: Device free human activity recognition through WiFi beacon-enabled camera," in *Proc. 2nd Workshop Phys. Anal.*, May 2015, pp. 7–12.
[52] S. Arshad, C. Feng, Y. Liu, Y. Hu, R. Yu, S. Zhou, and H. Li, "Wi-chase: A WiFi based human activity recognition system for sensorless environments," in *Proc. IEEE 18th Int. Symp. A World Wireless, Mobile Multimedia Netw. (WoWMoM)*, Jun. 2017, pp. 1–6.
[53] Y. Zeng, P. H. Pathak, and P. Mohapatra, "Analyzing shopper's behavior through WiFi signals," in *Proc. 2nd Workshop Phys. Anal.*, 2015, pp. 13–18.
[54] Q. Zhou, J. Xing, J. Li, and Q. Yang, "A device-free number gesture recognition approach based on deep learning," in *Proc. 12th Int. Conf. Comput. Intell. Secur. (CIS)*, 2016, pp. 57–63.
[55] O. Zhang and K. Srinivasan, "Mudra: User-friendly fine-grained gesture recognition using WiFi signals," in *Proc. 12th Int. Conf. Emerg. Netw. EXperiments Technol.*, Dec. 2016, pp. 83–96.
[56] Y. Zeng, P. H. Pathak, C. Xu, and P. Mohapatra, "Your AP knows how you move: Fine-grained device motion recognition through WiFi," in *Proc. 1st ACM Workshop Hot Topics Wireless*, 2014, pp. 49–54.
[57] A. Virmani and M. Shahzad, "Position and orientation agnostic gesture recognition using WiFi," in *Proc. 15th Annu. Int. Conf. Mobile Syst., Appl., Services*, Jun. 2017, pp. 252–264.
[58] D. Zhang, J. Wang, J. Jang, J. Zhang, and S. Kumar, "On the feasibility of Wi-Fi based material sensing," in *Proc. 25th Annu. Int. Conf. Mobile Comput. Netw.*, 2019, pp. 1–16.
[59] C. Wang, J. Liu, Y. Chen, H. Liu, and Y. Wang, "Towards in-baggage suspicious object detection using commodity WiFi," in *Proc. IEEE Conf. Commun. Netw. Secur. (CNS)*, May 2018, pp. 1–9.
[60] K. Wu, "Wi-metal: Detecting metal by using wireless networks," in *Proc. IEEE Int. Conf. Commun. (ICC)*, May 2016, pp. 1–6.
[61] B. Zhou, Z. Chen, Z. Gong, and R. Zhou, "Detection of suspicious objects concealed by walking pedestrians using WiFi," in *Proc. IEEE Wireless Commun. Netw. Conf. (WCNC)*, May 2020, pp. 1–6.
[62] A. Hanif, M. S. Chughtai, A. A. Qureshi, A. Aleem, F. Munir, M. Tahir, and M. Uppal, "Non-obtrusive detection of concealed metallic objects using commodity WiFi radios," in *Proc. IEEE Global Commun. Conf. (GLOBECOM)*, Dec. 2018, pp. 1–6.
[63] Y. Wu, G. Tian, and W. Liu, "Research on moisture content detection of wood components through Wi-Fi channel state information and deep extreme learning machine," *IEEE Sensors J.*, vol. 20, no. 17, pp. 9977–9988, Sep. 2020.
[64] W. Yang, X. Wang, A. Song, and S. Mao, "Wi-wheat: Contact-free wheat moisture detection with commodity WiFi," in *Proc. IEEE Int. Conf. Commun. (ICC)*, May 2018, pp. 1–6.
[65] H. Song, B. Wei, Q. Yu, X. Xiao, and T. Kikkawa, "WiEps: Measurement of dielectric property with commodity WiFi device—An application to ethanol/water mixture," *IEEE Internet Things J.*, vol. 7, no. 12, pp. 11667–11677, Dec. 2020.
[66] L. Alzubaidi, J. Zhang, A. J. Humaidi, A. Al-Dujaili, Y. Duan, O. Al-Shamma, J. Santamaría, M. A. Fadhel, M. Al-Amidie, and L. Farhan, "Review of deep learning: Concepts, CNN architectures, challenges, applications, future directions," *J. Big Data*, vol. 8, no. 1, pp. 1–74, Dec. 2021.
[67] Y. LeCun, L. Bottou, Y. Bengio, and P. Haffner, "Gradient-based learning applied to document recognition," *Proc. IEEE*, vol. 86, no. 11, pp. 2278–2324, Nov. 1998.
[68] S. Sun, B. Hu, Z. Yu, and X. Song, "A stochastic max pooling strategy for convolutional neural network trained by noisy samples," *Int. J. Comput. Commun. Control*, vol. 15, no. 1, pp. 1–9, Feb. 2020.
[69] A. Krizhevsky, I. Sutskever, and G. E. Hinton, "Imagenet classification with deep convolutional neural networks," in *Advances in Neural Information Processing Systems*, vol. 25, F. Pereira, C. Burges, L. Bottou, and K. Weinberger, Eds. Red Hook, NY, USA: Curran Associates, 2012.
[70] D. Berrar, "Cross-validation," in *Encyclopedia of Bioinformatics and Computational Biology*, S. Ranganathan, M. Gribskov, K. Nakai, and C. Schönbach, Eds. Oxford, U.K.: Academic, 2019, pp. 542–545.
[71] *Standard Test Methods for Laboratory Determination of Water (Moisture) Content of Soil and Rock by Mass*, Standard D2216–19, ASTM, 1998.
[72] M. Hofmann, "Support vector machines-kernels and the kernel trick," *Notes*, vol. 26, no. 3, pp. 1–16, 2006.

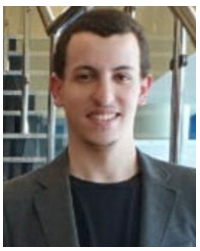

MOHAMED A. GACEM (Member, IEEE) received the B.Sc. degree in electrical engineering/electronics from Ajman University, United Arab Emirates, and the M.Sc. degree in electrical engineering from the American University of Sharjah. He has worked as a Graduate Teaching Assistant (GTA) and a Graduate Research Assistant (GRA) during his master's studies. His research interests include non-destructive evaluation using microwaves, deep learning, computer vision, and the IoT applications.

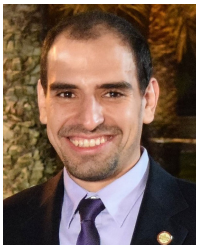

AMER S. ZAKARIA (Senior Member, IEEE) received the B.Sc. degree in electrical engineering from AUS, in 2006, the M.Sc. degree in microwave engineering from Technische Universität München, Germany, in 2007, and the Ph.D. degree in electrical engineering from the University of Manitoba, Winnipeg, Canada, in March 2012. From March 2012 to August 2014, he was a Postdoctoral Fellow with the Electromagnetic Imaging Laboratory, University of Manitoba. Since 2014, he has been with the Department of Electrical Engineering, AUS, where he is currently an Associate Professor. His research interests include biomedical imaging and applied electromagnetics. He is a Registered Professional Engineer with Engineers Geoscientists in Manitoba, Canada, and a member of the IEEE Honorary Society Eta-Kappa-Nu.

MAHMOUD H. ISMAIL (Senior Member, IEEE) received the B.Sc. degree (Hons.) in electronics and electrical communications engineering, the M.Sc. degree in communications engineering both from Cairo University, Egypt, in 2000 and 2002, respectively, and the Ph.D. degree in electrical engineering from the University of Mississippi, MS, USA, in 2006. From August 2000 to August 2002, he was a Research and Teaching Assistant at the Department of Electronics and Electrical Communications Engineering, Cairo University. From 2004 to 2006, he was a Research Assistant at the Center for Wireless Communications (CWC), University of Mississippi. He was also a Systems Engineering Consultant at Newport Media Inc. (currently a part of Microchip), Egypt Design Center, Cairo, from 2006 to 2014. He is currently a Full Professor at the American University of Sharjah, Sharjah, United Arab Emirates, and a Full Professor (on leave) at the Department of Electronics and Electrical Communications Engineering, Cairo University. His research interests include wireless communications with emphasis on performance evaluation of next-generation wireless systems and communications over fading channels. He is a member of Sigma Xi and Phi Kappa Phi. He was a recipient of the University of Mississippi Summer Assistantship Award in 2004 and 2005, the University of Mississippi Dissertation Fellowship Award in 2006, the University of Mississippi Graduate Achievement Award in electrical engineering in 2006, and the Best Paper Award presented at the tenth IEEE Symposium on Computers and Communications (ISCC 2005), La Manga del Mar Menor, Spain. He served as a reviewer for several refereed journals and conferences.

USMAN TARIQ (Member, IEEE) received the M.S. and Ph.D. degrees from the Electrical and Computer Engineering Department, University of Illinois at Urbana–Champaign (UIUC), in 2009 and 2013, respectively. He is currently a Faculty Member at the Department of Electrical Engineering, American University of Sharjah (AUS), United Arab Emirates. Before AUS, he worked as a Research Scientist with the Computer Vision Group, Xerox Research Center Europe, France. His research interests include computer vision, image processing, and machine learning, in general while facial expression recognition and face biometrics, in particular.

SHERIF YEHIA is the co-developer of the newly conductive concrete application for deicing operations. He has over 30 years of experience in research, construction material evaluation, and teaching. He has authored or coauthored more than 150 articles and technical reports published in internationally recognized journals/conference proceedings and holds two U.S. patents. He has participated in several funded research projects from various federal, state, and private sources. His research interests include behavior of reinforced and prestressed concrete, composite structures, special concrete, infrastructure management systems, engineering database management, and information technology.